ELSEVIER

Journal of Molecular Catalysis A: Chemical 121 (1997) 45–62

JOURNAL OF MOLECULAR CATALYSIS A: CHEMICAL

Theoretical studies of CO adsorption on H-ZSM-5 and hydrothermally treated H-ZSM-5

Holmann V. Brand, Antonio Redondo *, P. Jeffrey Hay

Theoretical Division, Los Alamos National Laboratory, Los Alamos, NM 87545, USA

Received 22 April 1996; accepted 26 November 1996

Abstract

The adsorption of CO on H-ZSM-5 and hydrothermally treated H-ZSM-5 is studied by means of quantum mechanical calculations. Good agreement with experimental FTIR data is established. The $Al(OH)_3$ dimer is found to account for the new bands that appear in the hydroxyl region of the FTIR spectra of H-ZSM-5 as a result of hydrothermal treatment. Effects of electron correlation (investigated through second-order Møller–Plesset perturbation and density-functional theory) are compared with Hartree–Fock results. Red shifts in the stretching frequency of bridging OH groups due to the CO interaction are best described by the density-functional approach. Frequency shifts are found to correlate with changes in local geometry.

Keywords: Zeolite; Brønsted acidity; CO adsorption; Dealumination; IR spectra; DFT; Theory; Hydroxyl frequencies; Scaling factors

1. Introduction

In this paper we aim at providing a theoretical interpretation and understanding of the observed experimental results of infrared (IR) spectroscopy on samples of H-ZSM-5 and the effects of hydrothermal (steaming) treatment and CO adsorption [1]. Hence, our calculations, reported herein, have focused on the vibrational frequencies of hydroxyl groups in zeolitic cluster models. As we shall see in the body of the paper, the calculations are in good agreement with those parts of the experiments that can be assigned from other, independent data. Furthermore, those parts of the experimental data that have been previously difficult to assign are interpreted on the basis of our calculations.

Specifically, we wish to address the following questions by means of quantum mechanical calculations: (a) What is the species that gives rise to the bands that appear in the hydroxyl region of the IR spectra of H-ZSM-5 upon hydrothermal (steaming) treatment? (b) what are the local geometries at the adsorption sites and the geometrical changes that accompany CO adsorption? And (c) what is the effect of electron correlation in the calculation of frequency shifts induced by CO adsorption?

This paper is organized as follows: Section 2 summarizes the experimental results that we are trying to model in the calculations; the details of the calculations are described in Section 3; Sec-

* Corresponding author.

1381-1169/97/$17.00 Copyright © 1997 Elsevier Science B.V. All rights reserved.
PII S1381-1169(96)00456-6

tion 4 contains a description of the results of the computations and comparison of the calculations with the experimental data; a discussion is presented in Section 5; finally, conclusions are summarized in Section 6.

2. Summary of experimental results

The infrared absorption experiments reported in Ref. [1] measured the vibrational infrared absorption on the OH and CO regions of the spectrum for untreated (ion-exchanged and then calcined) and hydrothermally treated samples of H-ZSM-5 in the absence and in the presence of adsorbed CO molecules. Such samples contain at least two forms of hydroxyl bonds: (a) silanols, Si–O–H, and (b) Brønsted acid sites, Si–(OH)–Al. A silanol site (Fig. 1a) is assumed

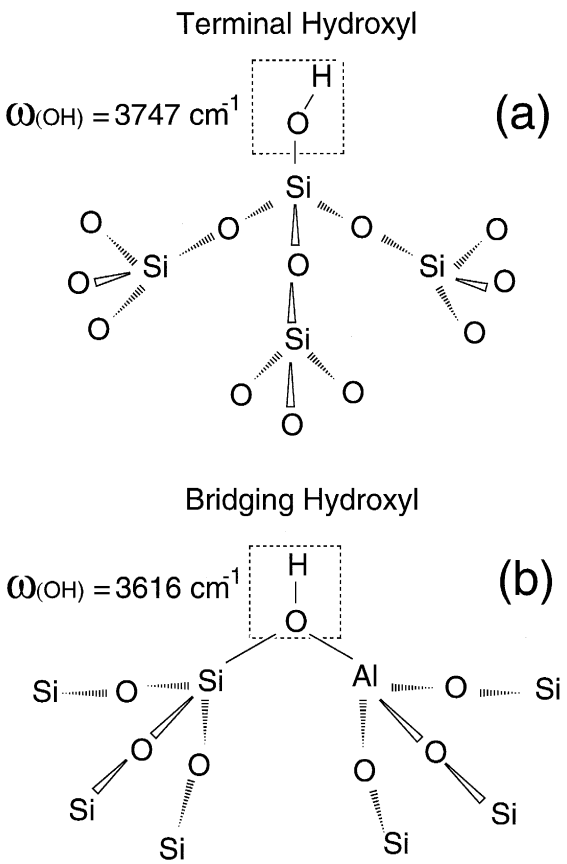

Fig. 1. Schematic drawings of hydroxyl groups in H-ZSM-5: (a) terminal hydroxyl group; (b) bridging hydroxyl group.

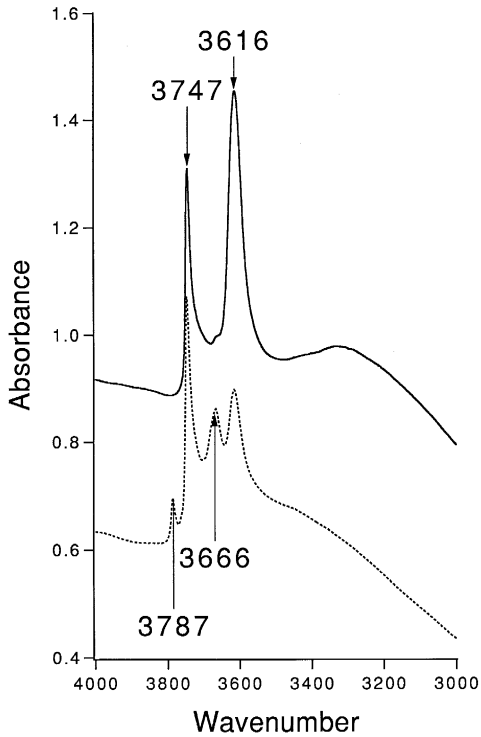

Fig. 2. Hydroxyl region FTIR spectra of H-ZSM-5: original sample (solid line); steamed sample (dashed line).

to be a defect site where an otherwise normal silicon–oxygen–silicon linkage is replaced by a silicon–oxygen–hydrogen terminal branch. A Brønsted acid site (Fig. 1b) consists of a proton bonded to a bridging oxygen atom which itself is bonded to one silicon and one aluminum atom.

The hydroxyl (OH) stretching vibrational region of the infrared spectrum in aluminum-substituted H-ZSM-5 (Fig. 2) consists of two intense absorption bands at 3616 cm^{-1} and 3747 cm^{-1} which have been previously assigned [1] to the OH stretch of Brønsted acid and silanol sites, respectively. In addition, there is a low intensity band at 3666 cm^{-1} which can, as explained by our work, be assigned to O–H stretching vibrational frequencies of bridging hydroxyl groups associated with aluminum atoms produced by the hydrothermal removal of framework aluminum during the sample calcination process.

As described in Ref. [1], when the H-ZSM-5

samples are steamed at over 800 K, the O–H stretching vibrational region of the infrared spectrum exhibits two strong absorption bands at 3666 cm^{-1} and 3787 cm^{-1}, in addition to the bands at 3616 cm^{-1} and 3747 cm^{-1} which were already present in the original unsteamed H-ZSM-5 (Fig. 2). The shape of the band at 3787 cm^{-1} is similar to that of the terminal hydroxyl at 3747 cm^{-1} whereas the shape of the 3666 cm^{-1} band resembles that of the bridging hydroxyl band at 3616 cm^{-1}. The two bands at 3666 cm^{-1} and 3787 cm^{-1} have also been observed in nanosized ZSM-5 samples by Zecchina et al. [2] and in steamed samples of zeolite β by Kiricsi et al. [3].

Upon adsorption of carbon monoxide on unsteamed H-ZSM-5 at 150 K, the OH stretching vibrational band at 3616 cm^{-1} disappears and a new broad band with a maximum at 3311 cm^{-1} is observed (Fig. 3). One can then conclude that the experiments show that the OH stretch of the bridging Si–(OH)–Al hydroxyl groups undergoes a red shift of about 300 cm^{-1} upon interaction with CO at 150 K. A similar shift of this band was observed at 77 K by Kustov et al. [4]. Adsorption of CO on steamed H-ZSM-5 samples also results in a 300 cm^{-1} red shift of the 3616 cm^{-1} band, as in the unsteamed samples. The band at 3666 cm^{-1} shifts down to 3463 cm^{-1}, which corresponds to an approximate red shift of 203 cm^{-1} (Fig. 3). The other two infrared features associated with OH bonds, the silanol band at 3747 cm^{-1} and the new band at 3787 cm^{-1}, do not appear to interact with the CO molecules at 153 K or above as their integrated infrared intensities remain unchanged after CO adsorption [1]. Similar shifts of the 3666 and 3616 cm^{-1} bands due to CO adsorption at 77 K were reported by Zecchina et al. [2].

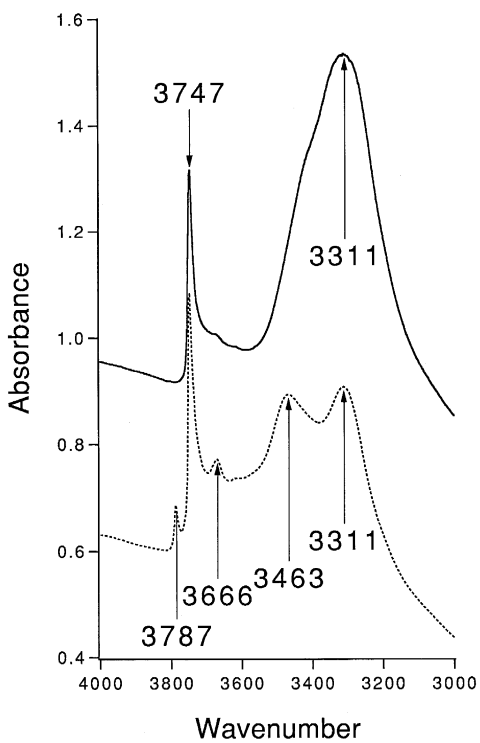

Fig. 3. Hydroxyl region FTIR spectra of H-ZSM-5 upon CO adsorption on the original sample (solid line) and the steamed sample (dashed line).

The CO stretching region of the infrared spectrum of the unsteamed sample exhibits [1] two strong absorption bands at 2140 cm^{-1} and 2173 cm^{-1} and a weaker band at 2230 cm^{-1}. The peak at 2140 cm^{-1} has been ascribed to CO physically adsorbed (condensed) in the pores of the zeolite and quickly disappears as the temperature of the sample is raised above 180 K. This band should be compared to the gas-phase absorption band of CO at 2143 cm^{-1} [5]. The most intense band at 2173 cm^{-1} corresponds to the stretching frequency of carbon monoxide molecules associated with the protons of the Brønsted acid sites. In the steamed sample, the CO stretching region shows a new feature at 2188 cm^{-1} in addition to the 2140, 2173 and 2230 cm^{-1} bands that were already present in the unsteamed samples. The feature at 2188 cm^{-1} has been thought to be associated with extra-framework aluminum species present in the zeolite channels [1].

3. Computational details

3.1. Cluster models

Calculations involving zeolite ZSM-5 reported herein have been performed using cluster

models. In such a model a fragment of the zeolite framework is cut out of the crystal and the resulting dangling bonds at the scission boundary of the cluster are saturated with either hydrogen atoms or OH groups. To model the terminal hydroxyl groups we have employed the silanol, H_3SiOH (Fig. 4a), and orthosilicic acid, $Si(OH)_4$ (Fig. 4b), molecules. These molecules have been used previously as cluster models of terminal hydroxyl groups in silica and zeolites [6,7]. The Brønsted acid site has been modeled using a $H_3Si(OH)AlH_3$ cluster (Fig. 5b) which has been used previously to calculate the stretching vibrational frequency of bridging OH groups [8,9]. In spite of their small size, these cluster models are known to lead to good agreement with the experimental results on the OH stretching vibrational frequencies of the terminal and bridging hydroxyl groups.

As noted in the section summarizing the experimental results, the hydroxyl region of the FTIR absorption spectrum of hydrothermally treated H-ZSM-5 exhibits two bands at 3787 and 3666 cm^{-1} that are thought to be associated with extra-framework aluminum. To model such groups we used an $Al(OH)_3$ molecule (Fig. 4c), as well as its corresponding dimer, $[Al(OH)_3]_2$ (Fig. 5a). The $Al(OH)_3$ monomer contains terminal hydroxyl groups and the dimer has both terminal and bridging hydroxyl species. It is worth pointing out that the $[Al(OH)_3]_2$ complex is not a zeolitic cluster but a molecular complex modeling the extra-framework aluminum and is, therefore, not subject to Lowenstein's rule that precludes formation of Al–O–Al bridges in zeolite frameworks. A previous computational study found that the calculated ^1H NMR chemical shift of the bridging OH groups in $[Al(OH)_3]_2$ is in the range assigned to hydroxyl groups of extra-framework material in dealuminated zeolites [10].

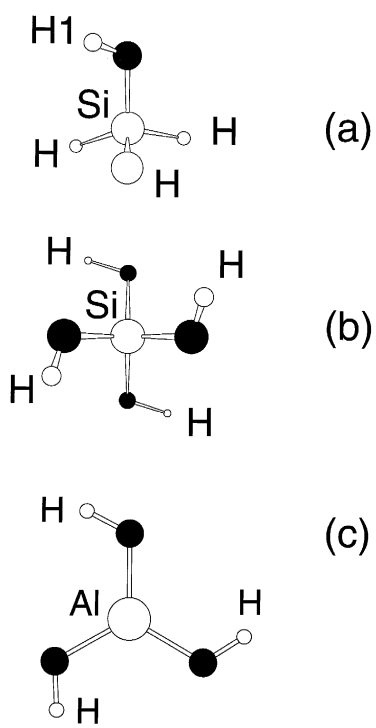

Fig. 4. Terminal hydroxyl cluster models: (a) H_3SiOH, (b) $Si(OH)_4$. (c) $Al(OH)_3$. Solid circles represent oxygen atoms.

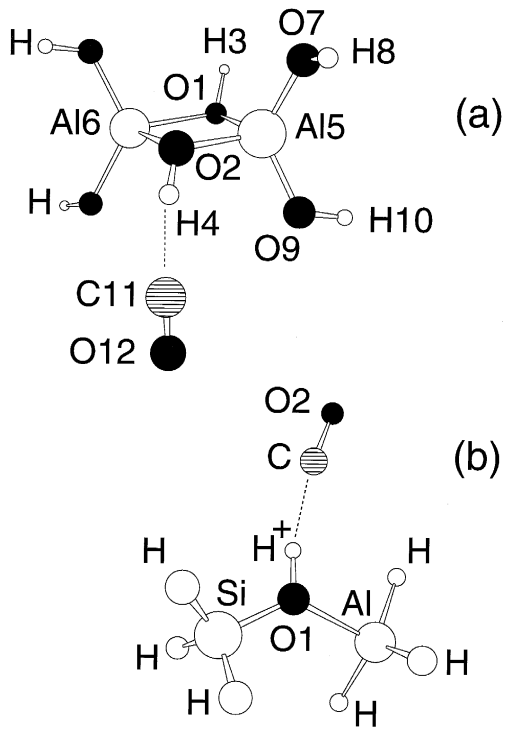

Fig. 5. CO adsorbed on a bridging hydroxyl of (a) extra-framework $Al(OH)_3$ dimer molecule and (b) $H_3Si(OH)AlH_3$ cluster model.

3.2. Wave functions and basis sets

We have employed several ab initio approaches to the solution of the Schrödinger equation for each cluster. The purpose of such a comparison is to establish a baseline of data that will allow us to calculate reliable vibrational frequencies for cluster models of zeolites. At the lowest level of approximation we used the Hartree–Fock (HF) wave function approach. This technique employs an uncorrelated, single-determinant wave function to describe the many-electron problem. We also report calculations where electronic correlation is included by means of second-order Møller–Plesset (MP2) perturbation theory [11]. In addition, we also performed density functional theory calculations using the gradient-corrected functional of Becke [12] for the exchange energy and the gradient-corrected functional of Lee, Yang and Parr [13] for the correlation energy. The density functional approximation, denoted by B-LYP, was implemented on atomic grids consisting of 50 radial shells and 194 angular points. The use of denser grids proved unnecessary and much more computationally expensive. The tables and the text clearly specify the type of calculation (i.e. HF, MP2 or B-LYP) that was carried out in each case. All the calculations were performed with the Gaussian 92 package [14].

An important aspect in the reliability of the calculations is the basis set used to expand the electron density. To obtain accurate results we have found that a good quality basis set is needed for calculations of vibrational frequencies. In the work reported herein we have employed two different basis sets composed of gaussian functions: The 6-31G* and 6-31G** sets of Pople and coworkers [15]. The 6-31G* basis set is constructed from the split-valence 6-31G basis by the addition of six d-type polarization functions on Si, Al and O atoms. The 6-31G** basis consists of the 6-31G* basis plus p-type polarization functions added on H atoms. Calculations employing the 6-31G* basis and the HF, MP2 and B-LYP methods will be denoted by HF/6-31G*, MP2/6-31G* and B-LYP/6-31G* in the data tables. The larger basis (i.e. 6-31G**) was used with the B-LYP method only and the results will be denoted by B-LYP/6-31G** in the data tables. Since the smaller basis (6-31G*) was employed with all three methods whereas the larger basis (6-31G**) was employed with the B-LYP method only, the discussion of our results will assume the smaller basis as implied unless otherwise explicitly stated.

3.3. Calculation of frequencies

In a systematic study, Johnson et al. [16] found that the binding energies and vibrational frequencies of a set of 32 first and second row small molecules calculated with density functional theory methods were in excellent agreement with experiment. Their comparison of results obtained with the 6-31G* basis set in both Hartree–Fock and density functional theory calculations showed that the density functional approach was superior. In particular, they found that the B-LYP approximation gave the best results. Their work also showed that harmonic frequencies calculated with the B-LYP method were closer to the experimental fundamental frequencies than to the experimental harmonic frequencies. These features of the B-LYP method are very useful in the assignment of experimental frequency bands and binding energies.

A recent study by Rauhut and Pulay [17] on the vibrational frequencies of 31 small molecules containing H, C, N, and O atoms showed that frequencies calculated with the B-LYP functionals and the 6-31G* basis set approximate the experimental values in a much more consistent fashion than the HF method with the same basis set. One approach employed to correct for the inherent errors in the calculated frequencies, as compared to experiment, is to use one or more of the experimental values to generate scaling factors to correct all the other calculated fre-

quencies [18]. This procedure is based on the observed trend that the error in the calculated vibrational frequencies is systematic within any particular computational method and can therefore be corrected by a transferable scaling factor determined empirically. In their study, Rauhut and Pulay also found that an overall uniform scaling factor for the B-LYP/6-31G* frequencies was close to unity and, thus, did not result in improved accuracy. On the other hand, the use of selective, multiple scaling factors that distinguish between the different kinds of internal coordinates of molecules containing common structural motifs did, in fact, lead to significant improvement in the agreement with experiment.

In the work reported herein we applied the HF, MP2, and B-LYP methods to the cluster models described above. Calculations with the B-LYP method and the larger basis contained p-type functions only on the bridging H in the case of the $H_3Si(OH)AlH_3$ zeolitic cluster and on all H atoms in all other cases. We calculated optimized geometric parameters of these molecular models by minimizing the total energy of the system. Then, at the optimum geometries, the corresponding harmonic frequencies were computed from the Hessian matrix of the system. Scaling factors, where appropriate, were then derived empirically for the OH and CO stretching vibrational frequencies by comparing with the experimental infrared bands for which we had solidly established assignments. Following the assumption of transferability, we assumed that the scaling factors for the terminal OH stretching harmonic frequencies for the $Al(OH)_3$ monomer and dimer are the same as those derived by comparing the OH stretching harmonic frequencies of the $Si(OH)_4$ cluster with the experimental band at 3747 cm^{-1}.

4. Results

4.1. Vibrational frequencies of terminal hydroxyl groups

Table 1 reports the calculated vibrational frequencies of the terminal hydroxyl groups, hereafter referred to as $\omega_{term}(OH)$; the appropriate scaling factors, denoted by σ; the scaled $\omega_{term}(OH)$ values and the corresponding experimental values. The scaling factors were determined by fitting the calculated frequencies $\omega_{term}(OH)$ of H_3SiOH and $Si(OH)_4$ to the experimental value of 3747 cm^{-1} of the silanol band (Fig. 2). The latter scaling factors were transferred to the corresponding $\omega_{term}(OH)$ calculations of the $Al(OH)_3$ monomer and dimer clusters. Note that the scaling factors for the

Table 1
Calculated stretching vibrational frequencies $\omega_{term}(OH)$ of terminal hydroxyl groups [a]

Species	HF/6-31G*		MP2/6-31G*		B-LYP/6-31G*		B-LYP/6-31G**		IR band [c]
	σ [b]	$\sigma\omega_{term}(OH)$	σ	$\sigma\omega_{term}(OH)$	σ	$\sigma\omega_{term}(OH)$	σ	$\sigma\omega_{term}(OH)$	
H_3SiOH	1	4145	1	3841	1	3658	1	3729	
	0.904	3747	0.976	3749	1.024	3746	1.005	3748	3747
$Si(OH)_4$	1	4140, 4145	1	3834, 3835, 3837	1	3657, 3659	1	3736, 3737	
	0.905	3747, 3751	0.977	3746, 3747, 3749	1.024	3745, 3747	1.003	3747, 3748	3747
$Al(OH)_3$	1	4176, 4179	1	3872, 3873	1	3679, 3680	1	3755, 3756	
	0.905	3779, 3782	0.977	3783, 3784	1.024	3767, 3768	1.003	3766, 3767	3787
$[Al(OH)_3]_2$	1	4188, 4190, 4191	1	3877, 3879	1	3694, 3696	1	3772, 3773, 3774	
	0.905	3790, 3792, 3793	0.977	3788, 3790	1.024	3783, 3785	1.003	3783, 3784, 3785	3787

[a] All frequencies are in cm^{-1}. Species shown in Fig. 4a–c and Fig. 5a.
[b] Scaling factors are denoted by σ and were determined by fitting the calculated frequencies of H_3SiOH and $Si(OH)_4$ to the experimental 3747 cm^{-1} IR band.
[c] High frequency IR bands in hydroxyl region of steamed H-ZSM-5 samples (Fig. 2).

H_3SiOH and $Si(OH)_4$ molecules are almost identical (to three decimal places) for each method, suggesting that the assumption of transferability of the scaling factor is appropriate for our calculations. Frequencies corresponding to a scaling factor of unity are the unscaled calculated $\omega_{term}(OH)$ frequencies.

As listed in Table 1, the 3747 cm^{-1} band is underestimated by the unscaled $\omega_{term}(OH)$ values calculated by B-LYP for the H_3SiOH and $Si(OH)_4$ clusters by 89 and 88–90 cm^{-1}, respectively, with the small basis and by only 18 and 10–11 cm^{-1}, respectively, with the larger basis. We note that the closest agreement between the unscaled $\omega_{term}(OH)$ values and the 3747 cm^{-1} band is accomplished by B-LYP with the larger basis. By comparision, unscaled $\omega_{term}(OH)$ values calculated by the HF and MP2 methods overestimate this band by as much as 398 cm^{-1} and 94 cm^{-1}, respectively.

Note also that similar results can be observed for the corresponding calculations of the unscaled $\omega_{term}(OH)$ values for the $Al(OH)_3$ and $[Al(OH)_3]_2$ clusters when compared to the experimental band at 3787 cm^{-1}. The B-LYP method with the larger basis produces unscaled $\omega_{term}(OH)$ values in closest agreement with the 3787 cm^{-1} band. The B-LYP method applied to the $Al(OH)_3$ and $[Al(OH)_3]_2$ clusters produces unscaled $\omega_{term}(OH)$ values that underestimate the 3787 cm^{-1} band by 107–108 cm^{-1} and 91–93 cm^{-1}, respectively, with the small basis and by 31–32 cm^{-1} and 13–15 cm^{-1}, respectively, with the larger basis. The HF and MP2 methods overestimate the 3787 cm^{-1} band by as much as 404 and 92 cm^{-1}, respectively.

The selective scaling factors for $\omega_{term}(OH)$ values shown in Table 1 are somewhat different from the uniform scaling factors recommended by Pople et al. [18] for frequencies calculated with the small basis used here. The selective scaling factors of 0.904 and 0.905 that we have found for our HF calculations on the H_3SiOH and $Si(OH)_4$ clusters are closer to unity than the uniform scaling factor of 0.8929 of Ref. [18]. Similarly, the values of $\sigma = 0.976$ and 0.977 we found for the MP2 calculations with the same basis set are also closer to unity than the uniform value of 0.9427 recommended by Pople et al. [18].

As shown in Table 1, excellent agreement with the 3787 cm^{-1} band is obtained by scaling the $\omega_{term}(OH)$ values of the $Al(OH)_3$ and $[Al(OH)_3]_2$ clusters with the selective scaling factors derived from fitting the calculated terminal hydroxyl frequencies of the $Si(OH)_4$ cluster to the 3747 cm^{-1} band. Using the selective scaling factors obtained from this fitting procedure results in values of $\omega_{term}(OH)$ that differ from the 3787 cm^{-1} band by at most 20 cm^{-1} in the case of $Al(OH)_3$ and by only 4 cm^{-1} in the case of the $[Al(OH)_3]_2$ complex. This excellent agreement strongly supports the transferability of the selective scaling factors.

4.2. Vibrational frequencies of bridging hydroxyl groups

The stretching vibrational frequency of the bridging hydroxyl groups, $\omega_{brid}(OH)$, of the $[Al(OH)_3]_2$ complex (Fig. 5a) are listed in Table 2. The unscaled $\omega_{brid}(OH)$ values in closest agreement with the experimental 3666 cm^{-1} band are the ones calculated with the B-LYP

Table 2
Calculated stretching vibrational frequencies $\omega_{brid}(OH)$ of bridging hydroxyl groups of $[Al(OH)_3]_2$ [a]

Species	HF/6-31G*	MP2/6-31G*	B-LYP/6-31G*	B-LYP/6-31G**	IR band [b]
$[Al(OH)_3]_2$	4116, 4118	3803	3645, 3647	3724, 3725	3666
$[Al(OH)_3]_2 \cdots CO$	4067	3687	3443	3490	3463
$\Delta\omega_{brid}(OH)$	−49, −51	−116	−202, −204	−234, −235	−203

[a] All frequencies in cm^{-1}. Species shown in Fig. 5a.
[b] Selected IR bands in hydroxyl region of original and steamed H-ZSM-5 samples (Figs. 2 and 3).

method and the smaller basis which underestimate this band by only 19–20 cm^{-1}. The use of the larger basis with the B-LYP method does not result in closer agreement. The unscaled HF and MP2 $\omega_{brid}(OH)$ values overestimate the 3666 cm^{-1} band by 450–452 cm^{-1} and 137 cm^{-1}, respectively.

Experimentally, upon adsorption of CO the 3666 cm^{-1} band undergoes a red shift of 203 cm^{-1} to the perturbed value of 3463 cm^{-1} (Fig. 3). Denoting by $\Delta\omega_{brid}(OH)$ the change (shift) in stretching frequency of the bridging OH bond in the $[Al(OH)_3]_2$ complex (Fig. 5a) induced by interaction with the CO molecule forming the $[Al(OH)_3]_2 \cdots CO$ complex, we see that the unscaled value of $\Delta\omega_{brid}(OH)$ calculated by the B-LYP method with the small basis is in closest agreement with experiment since it slightly underestimates the 3463 cm^{-1} band by 20 cm^{-1} and predicts a red shift of 202–204 cm^{-1}, in excellent agreement with the experimental value of 203 cm^{-1}. The B-LYP calculation with the larger basis results in an overestimate of the experimental shift by about 30 cm^{-1}. On the other hand, the HF and MP2 methods grossly underestimate the experimental shift by factors of about four and two, respectively. We note that the use of the uniform scaling factors 0.8929 and 0.9727 recommended by Pople for HF and MP2 frequencies [18] would further deteriorate agreement with the experimental frequency shift.

Table 3 lists the $\omega_{brid}(OH)$ frequencies for the calculations performed on the $H_3SiO(H)AlH_3$ cluster (Fig. 5b). The unscaled $\omega_{brid}(OH)$ value in closest agreement with the experimental 3616 cm^{-1} band is the one calculated with the B-LYP method and the smaller basis resulting in a 34 cm^{-1} overestimate of this band whereas employing the larger basis leads to a 110 cm^{-1} overestimate. The unscaled $\omega_{brid}(OH)$ values calculated with the HF and MP2 methods grossly overestimate the 3616 cm^{-1} band by 477 and 185 cm^{-1}. A similar performance is observed upon CO adsorption. the unscaled $\omega_{brid}(OH)$ value calculated for the $H_3Si(OH)AlH_3 \cdots CO$ complex with the B-LYP method and the smaller basis is the value closest to the experimental 3311 cm^{-1} band overestimating this band by 39 cm^{-1} whereas the use of the larger basis increases the overestimate to 71 cm^{-1}. The HF and MP2 approaches overestimate the 3311 cm^{-1} band by 717 and 352 cm^{-1}, respectively.

In comparison with the experimental 305 cm^{-1} red shift of the 3616 cm^{-1} band induced by the adsorption of CO, see Table 3, the closest agreement with the difference of unscaled $\omega_{brid}(OH)$ values of the $H_3SiO(H)AlH_3$ and $H_3Si(OH)AlH_3 \cdots CO$ clusters is afforded by the B-LYP method with the small basis which underestimates the experimental red shift by only 5 cm^{-1}. Using the larger basis set decreases the quality of the agreement. The $\Delta\omega_{brid}(OH)$ values calculated with the HF and MP2 methods grossly underestimate this experimental 305 cm^{-1} red shift by factors of 4 and 2, respectively. As noted above, the use of Pople scaling factors on the HF and MP2 $\Delta\omega_{brid}(OH)$

Table 3
Calculated stretching vibrational frequencies $\omega_{brid}(OH)$ of bridging hydroxyl groups of $H_3AlO(H)SiH_3$ [a]

Species	HF/6-31G*	MP2/6-31G*	B-LYP/6-31G*	B-LYP/6-31G**	IR band [b]
$H_3AlO(H)SiH_3$	4093	3801	3650 (3615) [c]	3726	3616
$H_3AlO(H)SiH_3 \cdots CO$	4028	3663	3350 (3310) [c]	3382	3311
$\Delta\omega_{brid}(OH)$	−65	−138	−300 (−305) [c]	−344	−305

[a] All frequencies in cm^{-1}. Species shown in Fig. 5b.
[b] Selected IR bands in hydroxyl region of H-ZSM-5 samples (Figs. 2 and 3).
[c] Calculated at geometries obtained by constraining the Si–O–Al angle to remain fixed at 141° during geometry optimization.

results does not improve the gross underestimates of the experimental red shift. We have thus verified the previously documented inability of the HF and MP2 methods to produce a realistic red shift in the stretching frequency of the bridging hydroxyl upon CO adsorption [9].

4.3. Vibrational frequencies of the CO molecule

Table 4 lists the stretching vibrational frequencies of the CO molecule, denoted by the symbol ω(CO), interacting with a bridging hydroxyl group of the $[Al(OH)_3]_2$ species and of the $H_3Si(OH)AlH_3$ zeolite cluster. The experimental [5] absorption band at 2143 cm^{-1} of free CO is grossly overestimated by the HF method and slightly underestimated by the MP2 and B-LYP methods. Also listed in Table 4 are the calculated changes in ω(CO) induced by the interaction with a bridging OH group. These changes, denoted by $\Delta\omega$(CO), are apparently less affected by the inclusion of electron correlation than the frequency shifts of the bridging OH groups are.

4.4. Carbon monoxide binding energies

Table 5 lists the calculated zero point and binding energies of CO interacting with a bridging hydroxyl group in the complexes $[Al(OH)_3]_2 \cdots CO$ (Fig. 5a) and $H_3Si(OH)AlH_3 \cdots CO$ (Fig. 5b). The zero-point energies are denoted by the subscript ZPE in the table; thus, $E_{ZPE}\{CO\}$ denotes the zero point energy of the isolated carbon monoxide molecule whereas $E_{ZPE}\{[Al(OH)_3]_2 \cdots CO\}$ denotes the zero point energy of the $Al(OH)_3]_2 \cdots CO$ complex. The trend in zero-point energies is to decrease upon inclusion of electron correlation. In particular, the B-LYP approach produces the smallest zero-point energies. However, the contribution of the zero point energy to the total binding energy of CO to the OH groups, denoted as ΔE_{ZPE}, is fairly constant and thus insensitive to electron correlation. For example, for the $[Al(OH)_3]_2 \cdots CO$ complex the quantity ΔE_{ZPE}, calculated using the expression $\Delta E_{ZPE} = E_{ZPE}\{CO\} + E_{ZPE}\{[Al(OH)_3]_2\} - E_{ZPE}\{[Al(OH)_3]_2 \cdots CO\}$, remains constant within 0.3 kcal/mol regardless of the method employed.

The electronic binding energy of CO on the bridging hydroxyl groups, denoted ΔE^e in Table 5, increases by a factor of at least 1.5 when electron correlation is included. For the $[Al(OH)_3]_2 \cdots CO$ complex the quantity ΔE^e is given by $\Delta E^e = E^e\{CO\} + E^e\{Al(OH)_3]_2\} - E^e\{[Al(OH)_3]_2 \cdots CO\}$, where E^e is the calculated total energy of the molecule or cluster at the optimum geometry. We note that the calculated values of the CO binding energy show good agreement (within 2 kcal/mol) with the experimental results [1] when electronic correlation is included, through either the MP2 or the B-LYP approaches.

4.5. Dimerization energy of $Al(OH)_3$

Table 6 lists the calculated zero point and dimerization energies of $Al(OH)_3$ (Fig. 5a and

Table 4
Calculated stretching vibrational frequencies of CO interacting with bridging hydroxyl groups of $[Al(OH)_3]_2$ and $H_3AlO(H)SiH_3$ [a]

Species	HF/6-31G*	MP2/6-31G*	B-LYP/6-31G*	B-LYP/6-31G**	IR band [b]
ω(CO)	2439	2119	2108	2108	2143
$[Al(OH)_3]_2 \cdots CO$	2458	2146	2139	2140	2188
$\Delta\omega$(CO)	+19	+27	+31	+32	+45
$H_3AlO(H)SiH_3 \cdots CO$	2474	2150	2143	2143	2173
$\Delta\omega$(CO)	+35	+31	+35	+35	+30

[a] All frequencies in cm^{-1}. Species shown in Fig. 5a and b.
[b] IR bands of CO adsorbed on original and steamed samples of H-ZSM-5 (from Ref. [1]).

Table 5
Calculated binding of CO to bridging hydroxyl groups of $[Al(OH)_3]_2$ and $H_3AlO(H)SiH_3$ [a]

Quantity	HF/6-31G*	MP2/6-31G*	B-LYP/6-31G*	B-LYP/6-31G**	Exp. [b]
$E_{ZPE}\{CO\}$	3.5	3.0	3.0	3.0	
$E_{ZPE}\{[Al(OH)_3]_2\}$	57.2	54.0	51.8	52.4	
$E_{ZPE}\{[Al(OH)_3]_2 \cdots CO\}$	61.6	58.1	55.6	56.2	
ΔE_{ZPE}	−0.9	−1.1	−0.8	−0.8	
ΔE^e	3.5	6.0	5.6	5.5	
$\Delta E^e + \Delta E_{ZPE}$	2.6	4.9	4.8	4.7	6.9
$E_{ZPE}\{H_3AlO(H)SiH_3\}$	40.6	39.2	36.9	37.0	
$E_{ZPE}\{H_3AlO(H)SiH_3 \cdots CO\}$	45.3	43.4	41.1	41.2	
ΔE_{ZPE}	−1.2	−1.2	−1.2	−1.2	
ΔE^e	3.6	6.1	6.4	6.4	
$\Delta E^e + \Delta E_{ZPE}$	2.4	4.9	5.2	5.2	7.7

[a] All energies in kcal/mol. Species shown in Fig. 5a and b.
[b] From CO adsorption on H-ZSM-5 and steamed H-ZSM-5 samples (Ref. [1]).

b). The zero point energies of the $Al(OH)_3$ monomer and dimer are denoted by $E_{ZPE}\{Al(OH)_3\}$ and $E_{ZPE}\{[Al(OH)_3]_2\}$ so that the contribution ΔE_{ZPE} of the zero point energy to the dimerization energy is given by $\Delta E_{ZPE} = 2E_{ZPE}\{Al(OH)_3\} - E_{ZPE}\{[Al(OH)_3]_2\}$.

As noted in the previous section, the ΔE_{ZPE} values calculated with the HF, MP2 and B-LYP methods agree within 0.2 kcal/mol suggesting insensitivity of ΔE_{ZPE} to electron correlation although the individual E_{ZPE} values decrease by as much as 5.4 kcal/mol upon inclusion of electron correlation.

The electronic dimerization energy ΔE^e, given by $\Delta E^e = 2E^e\{Al(OH)_3\} - E^e\{[Al(OH)_3]_2\}$, calculated with the MP2 method is 5.5 and 10.2 kcal/mol higher than the corresponding values calculated with the HF and B-LYP methods, respectively, using the same basis set. The ΔE^e values calculated with the B-LYP method and the two basis sets agree with each other within 0.3 kcal/mol. Hence, the electronic dimerization energy appears sensitive to the method employed. However, all methods predict the formation of the $[Al(OH)_3]_2$ molecule to be energetically stable by 59.9–70.1 kcal/mol with respect to the separated $Al(OH)_3$ monomers.

Table 6
Dimerization energy of $Al(OH)_3$ [a]

Quantity [b]	HF/6-31G*	MP2/6-31G*	B-LYP/6-31G*	B-LYP/6-31G**
$E_{ZPE}\{Al(OH)_3\}$	27.4	25.8	24.6	24.9
$E_{ZPE}\{[Al(OH)_3]_2\}$	57.2	54.0	51.8	52.4
ΔE_{ZPE}	−2.4	−2.4	−2.6	−2.6
ΔE^e	64.6	70.1	59.9	60.2
$\Delta E^e + \Delta E_{ZPE}$	62.2	67.7	57.3	57.6

[a] All energies in kcal/mol. Species shown in Fig. 4c and Fig. 5a.

4.6. Optimized geometries

The geometrical parameters of the optimum geometries for all the molecules and zeolitic clusters reported here are listed in Tables 7–11. Inclusion of electron correlation results in a general lengthening of covalent bonds and a shortening of hydrogen bonds. In particular, covalent bonds calculated with the B-LYP method are 0.01 Å longer than those calculated with the MP2 method, and covalent bonds calculated with the MP2 method are, in turn, 0.02 Å longer than those calculated with the HF method. Amongst the results obtained with the B-LYP method and the two basis sets, we note that the use of the larger basis leads to bonds that are 0.002–0.004 Å shorter than those obtained with the smaller basis. Angles are only weakly sensitive to inclusion of electron correlation. Comparing the HF and MP2 angles, the largest variation is only 7° with the dihedral

Table 7
Partial list of optimized geometrical parameters of H_3SiOH, $Si(OH)_4$ and $Al(OH)_3$ [a]

Parameter [b]	HF/ 6-31G*	MP2/ 6-31G*	B-LYP/ 6-31G*	B-LYP/ 6-31G**
H_3SiOH [b]				
r(O–Si)	1.647	1.672	1.684	1.683
r(O–H_1)	0.946	0.969	0.977	0.974
a(Si–O–H_1)	119.0	116.3	114.9	114.9
$Si(OH)_4$ [c]				
r(Si–O)	1.629	1.653	1.667	1.665
r(O–H)	0.947	0.970	0.978	0.974
a(Si–O–H)	117.1	114.1	112.9	113.3
$Al(OH)_3$ [d]				
r(O–H)	0.944	0.967	0.976	0.972
r(Al–O)	1.688	1.713	1.723	1.722
a(Al–O–H)	123.5	119.6	117.3	117.8

[a] Bond lengths in Ångström. Angles in degrees.
[b] Cluster parameters shown in Fig. 4a.
[c] Cluster parameters shown in Fig. 4b.
[d] Cluster parameters shown in Fig. 4c.

angles varying by less than 1°. Similarly, the MP2 and B-LYP angles differ by less than 3° and the dihedral angles remain virtually unchanged (within 1°).

The main changes in the geometry of the $[Al(OH)_3]_2$ molecule induced by the interaction of CO with a bridging OH group (Table 9) are a lengthening of the bridging OH bond and a shortening of the CO and O–Al bonds of the Al–O–Al bridge as well as some minor rotations in the dihedral angles of the terminal OH groups. The induced changes in bond lengths tend to be enhanced by the inclusion of electron correlation with the B-LYP method. The CO bond length, however, decreases only by a constant 0.003 Å for all the methods and basis sets considered.

The H ··· C hydrogen bond in the $[Al(OH)_3]_2$ ··· CO complex becomes shorter

Table 8
Optimized geometrical parameters of $[Al(OH)_3]_2$ [a]

Parameter [b]	HF/ 6-31G*	MP2/ 6-31G*	B-LYP/ 6-31G*	B-LYP/ 6-31G**
r(O$_1$–H$_3$)	0.950	0.973	0.979	0.975
r(O$_1$–Al$_5$)	1.847	1.869	1.881	1.880
r(Al$_5$–O$_7$)	1.703	1.727	1.736	1.734
r(O$_7$–H$_8$)	0.943	0.967	0.975	0.971
a(Al$_5$–O$_1$–Al$_6$)	97.7	96.3	96.5	96.5
a(O$_1$–Al$_5$–O$_2$)	82.3	83.7	83.5	83.5
a(O$_1$–Al$_5$–O$_7$)	104.7	103.1	103.5	103.7
a(O$_7$–Al$_5$–O$_9$)	121.8	123.7	123.4	123.4
a(Al$_5$–O$_7$–H$_8$)	124.9	120.9	118.2	118.8
a(O$_2$–O$_1$–H$_3$)	139.1	132.2	132.4	132.2
d(O$_2$–Al$_6$–Al$_5$–O$_7$)	101.3	102.2	101.9	101.5
d(Al$_6$–Al$_5$–O$_7$–H$_8$)	140.2	135.1	135.4	134.7

[a] Bond lengths in Ångström. Angles in degrees.
[b] Cluster parameters shown in Fig. 5a.

Table 9
Partial list of geometrical parameters of fully optimized $[Al(OH)_3]_2 \cdots CO$ [a]

Parameter [b]	HF/ 6-31G*	MP2/ 6-31G*	B-LYP/ 6-31G*	B-LYP/ 6-31G**
r(O$_1$–H$_3$)	0.949	0.973	0.979	0.975
r(O$_2$–H$_4$)	0.953	0.980	0.990	0.987
r(O$_1$–Al$_5$)	1.848	1.869	1.885	1.883
r(O$_2$–Al$_5$)	1.844	1.863	1.874	1.872
r(H$_4$–C$_{15}$)	2.356	2.136	2.062	2.039
r(Al$_5$–O$_7$)	1.703	1.728	1.737	1.735
r(Al$_5$–O$_9$)	1.707	1.732	1.741	1.739
r(O$_7$–H$_8$)	0.943	0.967	0.975	0.971
r(O$_9$–H$_{10}$)	0.944	0.967	0.975	0.972
r(C$_{15}$–O$_{16}$)	1.112	1.148	1.147	1.147
a(O$_2$–O$_1$–H$_3$)	139.6	133.0	131.9	132.4
a(O$_1$–O$_2$–H$_4$)	136.3	128.9	127.4	127.8
a(Al$_5$–O$_1$–Al$_6$)	97.2	95.6	95.5	95.4
a(Al$_5$–O$_2$–Al$_6$)	97.5	96.1	96.3	96.2
a(O$_2$–H$_4$–C$_{11}$)	149.9	152.9	157.8	157.8
a(O$_1$–Al$_5$–O$_2$)	82.6	84.2	84.1	84.2
a(H$_4$–C$_{11}$–O$_{12}$)	165.6	164.5	167.4	167.2
d(Al$_6$–O$_1$–Al$_5$–O$_2$)	0.0	0.0	0.0	0.0

[a] Bond lengths in Ångström. Angles in degrees.
[b] Cluster parameters shown in Fig. 5a.

Table 10
Partial list of geometrical parameters of fully optimized $H_3SiO(H)AlH_3$ [a]

Parameter [b]	HF/ 6-31G*	MP2/ 6-31G*	B-LYP/ 6-31G*	B-LYP/ 6-31G**
r(O–Al)	2.022	2.025	2.045	2.042
r(O–Si)	1.706	1.728	1.738	1.736
r(O–H^+)	0.951	0.973	0.979	0.975
a(Al–O–Si)	126.7	123.5	123.4	123.4
a(Al–O–H^+)	115.7	116.1	116.5	118.3
a(Si–O–H^+)	117.6	116.7	116.2	116.7
r(Al–H^+)	2.581	2.604	2.631	2.647
Alpha	1.0	20.4	20.9	13.1

[a] Bond lengths in Ångström. Angles in degrees.
[b] Cluster parameters shown in Fig. 5b.

Table 11
Partial list of geometrical parameters of fully optimized $H_3SiO(H)AlH_3 \cdots CO$ [a]

Parameter [b]	HF/ 6-31G*	MP2/ 6-31G*	B-LYP/ 6-31G*	B-LYP/ 6-31G**
$r(O_1–Al)$	2.008	2.008	2.032	2.031
$r(O_1–Si)$	1.700	1.719	1.724	1.723
$r(O_1–H^+)$	0.954	0.981	0.995	0.992
$r(Al–H^+)$	2.556	2.567	2.529	2.528
$r(H^+–C)$	2.286	2.100	1.992	1.972
$r(C–O_2)$	1.110	1.147	1.146	1.146
$a(Al–O_1–Si)$	127.3	124.5	128.2	127.9
$a(Al–O_1–H^+)$	114.5	113.9	108.4	108.5
$a(Si–O_1–H^+)$	118.2	117.2	117.2	117.6
$a(O_1–H^+–C)$	168.1	168.6	164.7	164.5
$a(H^+–C–O_2)$	176.2	174.1	171.8	171.9
$d(Al–O_1–H^+–C)$	0.0	2.9	0.0	0.0
$d(O_1–H^+–C–O_2)$	0.0	−1.4	−3.3	−1.2

[a] Bond lengths in Ångström. Angles in degrees.
[b] Cluster parameters shown in Fig. 5b.

upon inclusion of electron correlation. The $H \cdots C$ hydrogen bond is shortest when calculated with the B-LYP method especially with the use of the larger basis set. The $H \cdots C$ distances calculated with the HF and MP2 methods are longer than the corresponding B-LYP distance calculated with the same (smaller) basis. On the other hand, changes in the angles of the $[Al(OH)_3]_2 \cdots CO$ complex induced by electron correlation tend to be small. One of the largest changes occurs in the angle $OH \cdots C$ which only marginally increases by 3° in going from the HF result (149.9°) to that of the MP2 approximation and further increases by only 4.9° in going from the MP2 value to the B-LYP result. The angular parameters calculated with the B-LYP method are not sensitive to which of the two basis sets is employed.

Though, as mentioned above, angles do not seem sensitive to inclusion of electron correlation, a noticeable exception is, according to Table 10, the angle alpha between the bisector of the Si–O–Al angle in the Si–O–Al plane and the H atom of the bridging OH group, which appears to be very sensitive to electron correlation, increasing by as much as 19.4° upon inclusion of electron correlation in going from the HF value to the MP2 value. This angle then remains almost constant (within 0.5°) in going from the MP2 value to the B-LYP value. The same angle calculated with the B-LYP method and the larger basis set is smaller than the one calculated with the small basis set. A previous local spin density functional study found the proton forming an angle of 10° with the Si–O–Al plane [19].

The dependence of the geometrical parameters of the $H_3Si(OH)AlH_3$ cluster on the method employed are consistent with the patterns noted for the other clusters. Bonds calculated with the B-LYP and MP2 methods are longer than those calculated with the HF method in the order B-LYP > MP2 > HF. Likewise, the distance between the Al atom and the H atom (proton) of the bridging OH group follows the same trend. Using the B-LYP method with the larger basis results in an even longer $H^+ \cdots Al$ distance. These calculated values (Table 10) can be compared with the experimental range of 2.40–2.52 Å for the $H^+ \cdots Al$ distance in H-ZSM-5 estimated from NMR measurements [20]. Clearly all the methods overestimate the $H^+ \cdots Al$ distance. This discrepancy is perhaps related to the dynamical nature of the NMR measurements whereas the calculated geometries are static at the minimum of the energy surface. It should be pointed out that, according to the B-LYP method and the small basis, constraining the $Al–O–H^+$ angle to remain at 96.5° while optimizing all the other geometrical parameters of the $H_3Si(OH)AlH_3$ cluster, results in a structure with a $H^+ \cdots Al$ distance of 2.400 Å, an alpha angle of 49.5° and an energy that is only 0.6 kcal/mol above the energy minimum. Similarly, constraining the proton to remain in the Si–O–Al plane during the optimization results in a structure with a $H^+ \cdots Al$ distance of 2.655 Å and an energy that is less than 0.1 kcal/mol above the energy minimum. Hence, motion of the proton along the $Al–O–H^+$ and alpha angles costs very little energy and the NMR measurement of the $H^+ \cdots Al$ distance can therefore be considered a dynamical average.

The geometrical changes in the $H_3Si(OH)AlH_3 \cdots CO$ complex induced by the interaction with the CO molecule are a lengthening of the bridging OH bond, a shortening of the Si–O, Al–O and CO bonds and $H^+ \cdots Al$ distance, a small decrease in the Si–O–Al angle and a slight rotation in the dihedral angles of the saturating H atoms. These variations in the distances and angles due to the CO interaction tend to be augmented by the inclusion of electron correlation. The B-LYP method predicts the largest increase in the OH bond which is about 5 and 2 times greater than the increase predicted by the HF and MP2 methods, respectively. The $H \cdots C$ hydrogen bond is shortest when calculated with the B-LYP method. The HF and MP2 methods predict the $H \cdots C$ hydrogen bond to be longer than the one calculated with the B-LYP method and the same basis. The $H \cdots C$ hydrogen bond calculated with the B-LYP method and the larger basis is shorter than the one calculated with the smaller basis. The decrease in the CO bond length due to the CO interaction with the bridging OH group of the Brønsted site cluster is, on the other hand, found to be constant (0.004 Å) regardless of the method employed. In the presence of the CO molecule the Si–O–Al angle decreases only slightly. The largest decrease (4.8°) in the Si–O–Al angle is calculated with the B-LYP method whereas the HF and MP2 methods leave the Si–O–Al angle unchanged within 1°.

5. Discussion

5.1. Selective scaling and dealumination complex

Scaling the $\omega_{term}(OH)$ values of $[Al(OH)_3]_2$ with the selective scaling factors derived by fitting the $\omega_{term}(OH)$ values of the $Si(OH)_4$ cluster to the 3747 cm^{-1} band, results in scaled $\omega_{term}(OH)$ values of $[Al(OH)_3]_2$ that agree with the 3787 cm^{-1} band within 4 cm^{-1} when the B-LYP method is employed and within 6 and 3 cm^{-1} when using the HF and MP2 methods. As mentioned above, this excellent agreement with experiment strongly supports the transferability of the selective scaling factors. In addition we note that since the scaled $\omega_{term}(OH)$ values calculated with the B-LYP method and the smaller and larger basis sets agree with each other, the use of scaling factors renders the more expensive calculation of $\omega_{term}(OH)$ with the larger basis unnecessary.

The $\omega_{brid}(OH)$ and $\Delta\omega_{brid}(OH)$ of $[Al(OH)_3]_2$ calculated with the B-LYP method and the small basis agree with the measured 3666 cm^{-1} band (within 19–21 cm^{-1}) and the 203 cm^{-1} red shift (within 1 cm^{-1}) that this band undergoes upon CO adsorption (Table 2). Such close agreement between theory and experiment corroborates the likelihood of the $[Al(OH)_3]_2$ molecule as an extra-framework aluminum-containing species that results from the hydrothermally induced dealumination of the zeolite. This close agreement also suggests that the scaling factor for $\omega_{brid}(OH)$ calculated with the B-LYP method may indeed be one. It is also encouraging that an independent study by Fleischer et al. [10] found that the ^1H NMR chemical shift of the bridging protons in the $[Al(OH)_3]_2$ molecule lies in the range assigned to hydroxyl groups associated with extra-framework material in dealuminated zeolites.

5.2. Brønsted bridging hydroxyl groups

The $\Delta\omega_{brid}(OH)$ value of $H_3Si(OH)AlH_3$ caused by the CO interaction is in closest agreement with the experimental shift of 305 cm^{-1} when the computational method employed is the B-LYP approximation with the small basis set. This close agreement suggests that the selective scaling factor for $\omega_{brid}(OH)$ values calculated with the B-LYP approximation with the small basis set is indeed close to unity. Considering the this close agreement, one may therefore wonder why the $\omega_{brid}(OH)$ values of the $H_3Si(OH)AlH_3$ and $H_3Si(OH)AlH_3 \cdots CO$ calculated with the same method and basis over estimate the 3616 and 3311 cm^{-1} bands.

Since it has been suggested that the stretching frequency of the bridging hydroxyl decreases with increasing Si–O–Al angle [21], we attempted to estimate the Si–O–Al angular dependence of ω_{brid}(OH) with the B-LYP method and the small basis set at various Al–O–Si angles by calculating all the normal mode frequencies of the $H_3Si(OH)AlH_3$ cluster at optimized geometries for which the Si–O–Al angle had been kept fixed at particular values (130°–148°) during the optimization. The results, listed in Table 12, clearly show that ω_{brid}(OH) does indeed decrease with increasing Si–O–Al angle. Assuming that the selective scaling factor for ω_{brid}(OH) is indeed unity, these estimates suggest that Brønsted sites in H-ZSM-5 occur at Si–O–Al angles close to 140° which are below the range of Si–O–Si angles in ZSM-5 derived from X-ray diffraction, namely 145° to 175°. In particular, the ω_{brid}(OH) value calculated at an Si–O–Al angle of 141° turned out to be 3615 cm^{-1} which is in very close agreement with the experimental 3616 cm^{-1} band. A calculation of the normal modes of the $H_3Si(OH)AlH_3 \cdots CO$ complex with the same method and basis set at an optimized geometry in which the Al–O–Si angle was kept fixed at 141° during the optimization, resulted in a perturbed ω_{brid}(OH) value of 3310 cm^{-1} in very close agreement with the 3311 cm^{-1} band. The estimated shift in ω_{brid}(OH) of the $H_3Si(OH)AlH_3$ cluster calculated with the B-LYP method and the small basis set at an Si–O–Al angle of 141° is therefore 305 cm^{-1} which coincides with the experimental 305 cm^{-1} value. It therefore appears that the zeolite framework imposes geometrical constraints on the Si–(OH)–Al bridge such that the Si–O–Al angle in the zeolite is greater than that of the fully optimized $H_3Si(OH)AlH_3$ cluster.

Table 12
Dependence of stretching vibrational frequencies ω_{brid}(OH) of $H_3AlO(H)SiH_3$ cluster on Si–O–Al angle [a]

Si–O–Al angle	B-LYP/6-31G*
123.4	3650
130	3641
134	3632
138	3624
139	3622
140	3619
141	3615
142	3611
144	3603
146	3594
148	3584

[a] All frequencies in cm^{-1}. Angles in degrees.

As listed in Table 4, the experimentally observed frequency shift that the CO molecule undergoes when adsorbed at 3666 cm^{-1} OH groups is 15 cm^{-1} larger than when adsorbed at 3616 cm^{-1} OH groups whereas the trend in the frequency shift calculated with the B-LYP method and the small basis at the fully optimized $[Al(OH)_3]_2 \cdots CO$ complex is actually 4 cm^{-1} smaller than at the fully optimized $H_3Si(OH)AlH_3 \cdots CO$ complex. Wishing to understand this discrepancy, we looked in detail at the optimized geometry of the $[Al(OH)_3]_2 \cdots CO$ complex and noticed that the distance between the carbon atom of the adsorbed CO molecule and two oxygen atoms of terminal OH groups was about 3.3 Å and it was therefore conceivable that these two terminal OH groups were donating charge to the CO thereby reducing its frequency shift $\Delta\omega$(CO).

In order to test the effect of nearby terminal OH groups on the frequency shift of the CO molecule adsorbed at a bridging OH group in the $[Al(OH)_3]_2 \cdots CO$ complex, we restricted the CO molecule to remain collinear with the bridging OH group on which it is adsorbed (i.e. according to Fig. 5a, the angles O_2–H_4–C_{11} and H_4–C_{11}–O_{12} were kept fixed at 180°) and optimized all the other geometrical parameters. The structure optimized with this constraint was only 0.6 kcal/mol higher in energy than the fully optimized structure thereby suggesting that it is an energetically feasible structure at the temperature at which the experiments were conducted. The frequency shift of CO at this new structure is 35 cm^{-1} which is 4 cm^{-1} higher than the one calculated at the fully optimized structure. We also noticed that in the structure

optimized with the collinearity constraint, the distance between the carbon atom of the adsorbed CO and the two oxygen atoms of the closest terminal OH groups is 0.4 Å longer than in the fully optimized structure (i.e. without any constraints). It therefore appears that the proximity between the CO molecule and two nearby terminal OH groups in the fully optimized structure is what causes the blue shift in the $[Al(OH)_3]_2 \cdots CO$ complex to be smaller than in the $H_3Si(OH)AlH_3 \cdots CO$.

It is worth noting that, according to the B-LYP method and the small basis, the stretching frequency of CO, in the $H_3Si(OH)AlH_3 \cdots CO$ complex with the Al–O–Si angle kept fixed at 141° is 2137 cm^{-1} and the corresponding blue shift $\Delta\omega(CO)$ is 29 cm^{-1}. Therefore, comparing the frequency shift of CO in the $[Al(OH)_3]_2 \cdots CO$ complex with the CO constrained to remain linear at the bridging OH group, namely 35 cm^{-1}, with the frequency shift of CO in the $H_3Si(OH)AlH_3 \cdots CO$ complex with the Al–O–Si angle fixed at 141°, namely 29 cm^{-1}, we see agreement between the calculated trend and the experimentally observed trend in blue shift of CO upon adsorption at 3666 cm^{-1} OH groups being larger than at 3616 cm^{-1} OH groups.

During the writing of our present work, Farnworth and O'Malley have published a paper [22] in which they present an alternative way of including anharmonicity corrections in the stretching frequency of the terminal and bridging OH groups of the cluster models H_3SiOH and $H_3Al(OH)SiH_3$ and their interaction with CO. They employ the B-LYP and Becke3-LYP approximations [23]. Their approach does not make use of scaling factors but an anharmonicity constant obtained by fitting the energy profile along the OH bond to a Morse potential function. In their density-functional calculations, Farnworth and O'Malley do not take into account the dependence of the stretching frequency of the bridging OH group on the Si–O–Al angle which had been previously investigated by O'Malley and Dwyer [21] with the Hartree–Fock method. According to our Table 12, the stretching frequency of the bridging OH group calculated with B-LYP decreases with increasing Si–O–Al angle. Therefore, since the anharmonic effects considered by Farnworth and O'Malley were calculated at the narrow Si–O–Al angle of the optimized $H_3Al(OH)SiH_3$ cluster, their 'corrected' values for OH are likely to be biased.

5.3. Correlation between geometry, frequency shifts and binding

In agreement with the work of Johnson et al. [16], we find that inclusion of electron correlation lengthens covalent bonds especially with the B-LYP method which results in the longest bonds. For example, the bond lengths of the bridging OH groups in the $[Al(OH)_3]_2$ and $H_3Si(OH)AlH_3$ complexes calculated with the B-LYP method are longer than those calculated with the MP2 method which are in turn longer than those calculated with the HF method. However, using the larger basis set and the B-LYP method results in OH bond lengths slightly shorter than those calculated with the smaller basis set and the same method (B-LYP).

Comparing the $H_3Si(OH)AlH_3 \cdots CO$ and $[Al(OH)_3]_2 \cdots CO$ complexes, we note that the former has a shorter $H \cdots C$ hydrogen bond, undergoes a greater OH bond length elongation and a greater OH stretching frequency shift, $\Delta\omega_{brid}(OH)$, than the latter. Inclusion of electron correlation shortens the $H \cdots C$ bonds in both complexes and increases the binding energy of CO on the bridging OH groups. Amongst the electron correlation methods (MP2 and B-LYP) using the same basis, the $H \cdots C$ bonds calculated with the B-LYP method are shorter. The shortest $H \cdots C$ distances and greatest OH bond elongations are obtained with the B-LYP method. The lengthening of the OH bonds is particularly enhanced in the B-LYP calculations with the larger basis set. These increases in the OH bond length correlate with the trend found in the induced red shifts, $\Delta\omega_{brid}(OH)$, calculated with the B-LYP method being about 4 and

2 times larger than the corresponding red shifts calculated with the HF and MP2 methods, respectively.

In contrast to the lengthening of the OH bond and the shortening of the H · · · C hydrogen bond so evident upon inclusion of correlation, the shortening of the CO bond length is, on the other hand, fairly constant. In the $[Al(OH)_3]_2$ · · · CO complex the CO bond length decreases by 0.002 Å according to the HF method and 0.003 Å according to the MP2 and B-LYP methods. These small decreases in the CO bond length correlate with the blue shift, $\Delta\omega$(CO), in the stretching vibrational frequency of CO induced by the H · · · C interaction. In the $[Al(OH)_3]_2$ · · · CO complex the decrease in CO bond length and the blue shift $\Delta\omega$(CO) calculated with the HF method are both about one half the corresponding decreases calculated with the B-LYP method and the same basis set. Further, the MP2 blue shift is closer to the B-LYP value than to the HF value, indicating that the common 0.003 Å decrease in CO bond length calculated with the electron correlation methods (MP2 and B-LYP) results in similar blue shift values. In the $H_3Si(OH)AlH_3$ · · · CO complex, the CO bond length decreases by the same amount, 0.004 Å, according to all the methods (HF, MP2 and B-LYP) and the corresponding blue shifts thus agree with each other within a few wave numbers.

For future reference, all the vibrational frequencies of the $[Al(OH)_3]_2$ molecule calculated with the B-LYP method and the small basis are listed in Table 13.

Table 13
B-LYP/6-31G* vibrational frequencies of $[Al(OH)_3]_2$ [a]

Mode (symmetry)	Frequency [b]
Al–Al–O_{term} bend (B_u)	67
Al–O_{term} twist (A_u)	101
OH_{term} twist (B_g)	151
O_{brid}–Al–O_{brid} bend (A_g)	161
OH_{term} twist (B_u)	172
Al–Al–O_{term} bend (B_g)	174
O_{brid}–Al–O_{term} bend (B_u)	205
Al–O_{term} twist (A_g)	211
Al–O_{term}–H bend (A_u)	234
Ring torsion (B_g)	259
O_{brid} bend (Bu)	288
OH_{term} twist (A_u)	293
OH_{term} twist (A_g)	294
Al–O_{brid}–Al bend (A_g)	367
Al–O_{brid} stretch (B_g)	477
O_{brid}–H bend (A_g)	512
O_{brid}–H bend (B_u)	519
Al–O_{brid} stretch (A_u)	541
Al–O_{brid} stretch (B_u)	595
O_{brid}–H bend (A_g)	640
Al–O_{term}–H bend and Al–O_{term} stretch (A_u)	667
Al–O_{term}–H bend and Al–O_{term} stretch (A_g)	687
Al–O_{term}–H bend (B_g)	688
Al–O_{term}–H bend (B_u)	720
Al–O_{term} stretch (A_u)	773
Al–O_{term} stretch (A_g)	811
Al–O_{term} stretch (B_g)	850
Al–O_{term} stretch (B_u)	886
O_{brid}–H bend (A_u)	907
O_{brid}–H bend (B_g)	923
O_{brid}–H stretch (A_g)	3645
O_{brid}–H stretch (B_u)	3647
O_{term}–H stretch (B_g)	3694
O_{term}–H stretch (B_u)	3694
O_{term}–H stretch (A_u)	3696
O_{term}–H stretch (A_g)	3696

[a] Geometry optimized in C_{2H} symmetry.
[b] All frequencies in cm^{-1}.

6. Conclusions

The following conclusions can be derived from the present work:

(1) The two experimental bands at 3787 and 3666 cm^{-1} that appear in the OH region of the IR spectrum of hydrothermally treated H-ZSM-5 samples can be assigned to the stretching vibrational frequencies of terminal and bridging OH groups in the Al-containing species $[Al(OH)_3]_2$ which is formed as a result of dealumination of the zeolite framework upon steaming.

(2) The use of selective scaling factors on stretching frequencies of terminal OH groups, ω_{term}(OH), leads to excellent agreement with experiment. The selective scaling factors for ω_{term}(OH) derived by fitting the calculated ω_{term}(OH) of the $Si(OH)_4$ cluster to the 3747 cm^{-1} band, resulted in excellent agreement between the scaled ω_{term}(OH) of the $[Al(OH)_3]_2$

cluster and the measured 3787 cm^{-1} band. The shifts in stretching frequencies of bridging OH groups, $\Delta\omega_{brid}(OH)$, of the $[Al(OH)_3]_2 \cdots CO$ and $H_3Si(OH)AlH_3 \cdots CO$ complexes calculated with the B-LYP method and the 6-31G* basis set resulted in closest agreement (1–5 cm^{-1}) with the measured 203 and 305 cm^{-1} red shifts that the 3666 and 3616 cm^{-1} bands undergo, respectively, upon interaction with the CO molecule. On the other hand, both HF and MP2 methods grossly underestimate the red shifts experienced by the OH groups upon CO adsorption.

(3) The red shifts in the OH stretching vibrational frequencies induced by the H···C interaction of CO with a bridging OH group in the $[Al(OH)_3]_2 \cdots CO$ and $H_3Si(OH)AlH_3 \cdots CO$ complexes are associated with changes in their corresponding OH bond lengths. Inclusion of electron correlation results in shorter non-covalent H···C bonds and longer covalent OH bonds involved in the CO adsorption. These changes in H···C and OH bond lengths are particularly enhanced with the B-LYP method and are accompanied by red shifts in the calculated $\omega_{brid}(OH)$ that are closest to the experimental 203 and 305 cm^{-1} red shifts when the B-LYP method is used with the 6-31G* basis set.

(4) The calculated blue shift in $\omega(CO)$ caused by the interaction of the CO molecule with the Brønsted proton is related to the decrease in CO bond length. The greater the decrease in CO bond length the larger the blue shift in $\omega(CO)$. In the $[Al(OH)_3]_2 \cdots CO$ complex, the magnitudes of both the blue shift in $\omega(CO)$ and the decrease in CO bond length calculated with the Hartree–Fock method are about one half of the corresponding values calculated with the B-LYP method and the same basis set (6-31G*). In the $H_3Si(OH)AlH_3 \cdots CO$ complex, the decrease in CO bond length is constant (0.004 Å) according to the HF, MP2 and B-LYP methods and the corresponding blue shifts in $\omega(CO)$ are thus fairly constant (within 4 cm^{-1}).

(5) The angle between the bisector of the Si–O–Al angle in the Si–O–Al plane and the H atom (proton) of the bridging OH group of the $H_3Si(OH)AlH_3$ cluster is very sensitive to inclusion of electron correlation. Under no symmetry constraints, the proton deviates from the Si–O–Al plane by as much as 20.4–20.9° upon inclusion of electron correlation with the MP2 and B-LYP methods with the 6-31G* basis set. By comparison, the HF method with the same basis set predicts the proton to remain in the Si–O–Al plane (within less than 1°) leading to C_S symmetry in the $H_3Si(OH)AlH_3$ cluster. The B-LYP method with the larger basis set (6-31G**) predicts this angle to be 13.1°.

(6) In agreement with the work of Johnson et al. [16], bond lengths are found to increase upon inclusion of electron correlation in the order HF < MP2 < B-LYP with the 6-31G* basis set. Comparison of bond lengths calculated with the B-LYP method and both 6-31G* and 6-31G** basis sets, shows that the 6-31G** basis set results in shorter OH bonds and shorter H···C hydrogen bonds.

Acknowledgements

This work was partly carried out under the auspices of the US Department of Energy, Office of Industrial Technologies. We gratefully acknowledge insightful conversations with Dr. Richard L. Martin. We also thank Dr. Janos Szanyi and Dr. Mark T. Paffett for kindly providing the FTIR spectra.

References

[1] J. Szanyi and M.T. Paffett, Microporous Mater. 7 (1996) 201, and references therein.
[2] A. Zecchina, S. Bordiga, G. Spoto, D. Scarano, G. Petrini, G. Leofanti, M. Padovan and C. Otero-Arean, J. Chem. Soc. Faraday Trans. 88 (1992) 2959.
[3] I. Kiricsi, C. Flego, G. Pazzuconi, W.O. Parker Jr., R. Millini, C. Perego and G. Bellussi, J. Phys. Chem. 98 (1994) 4627, and references therein.
[4] L.M. Kustov, V.B. Kazansky, S. Beran, L. Kubelkova and P. Jiru, J. Phys. Chem. 91 (1987) 5247.

[5] K.P. Huber and G. Herzberg, Constants of Diatomic Molecules (Van Nostrand Reinhold, New York, 1979) p. 166.
[6] J. Sauer, Chem. Rev. 89 (1989) 199.
[7] P. Ugliengo, V.R. Saunders and E. Garrone, J. Phys. Chem. 93 (1989) 5210.
[8] J. Sauer, J. Phys. Chem. 91 (1987) 2315; J. Dwyer and S. Bates, J. Phys. Chem. 97 (1993) 5897; J. Mol. Struct. (Theochem.) 303 (1994) 65.
[9] J. Sauer, P. Ugliengo, E. Garrone and V.R. Saunders, Chem. Rev. 94 (1994) 2095.
[10] U. Fleischer, W. Kutzelnigg, A. Bleiber and J. Sauer, J. Am. Chem. Soc. 115 (1993) 7833.
[11] C. Møller and M.S. Plesset, Phys. Rev. 46 (1934) 618; J.S. Binkley and J.A. Pople, Int. J. Quantum Chem. 9 (1975) 229.
[12] A.D. Becke, Phys. Rev. A 38 (1988) 3098.
[13] C. Lee, W. Yang and R.G. Parr, Phys. Rev. B 37 (1988) 785.
[14] M.J. Frisch, G.W. Trucks, H.B. Schlegel, P.M.W. Gill, B.G. Johnson, M.W. Wong, J.B. Foresman, M.A. Robb, M. Head-Gordon, E.S. Replogle, R. Gomperts, J.L. Andres, K. Raghavachari, J.S. Binkley, C. Gonzalez, R.L. Martin, D.J. Fox, D.J. Defrees, J. Baker, J.J.P. Stewart and J.A. Pople, Gaussian 92/DFT, Revision G.1 (Gaussian, Inc., Pittsburgh, PA, 1993).
[15] W.J. Hehre, L. Radom, P.V.R. Schleyer and J.A. Pople, Ab Initio Molecular Orbital Theory (Wiley-Interscience, New York, 1986) p. 82, and references therein.
[16] B.G. Johnson, P.M.W. Gill and J.A. Pople, J. Chem. Phys. 98 (1993) 5612.
[17] G. Rauhut and P. Pulay, J. Phys. Chem. 99 (1995) 3093.
[18] J.A. Pople, A.P. Scott, M.W. Wong and L. Radom, Isr. J. Chem. 33 (1993) 345.
[19] S.J. Cook, A.K. Chakraborty, A.T. Bell and D.N. Theodorou, J. Phys. Chem. 97 (1993) 6679.
[20] M. Hunger, D. Freude, D. Fenzke and H. Pfeifer, Chem. Phys. Lett. 191 (1992) 391; N.P. Kenaston, A.T. Bell and J.A. Reimer, J. Phys. Chem. 98 (1994) 894.
[21] P.J. O'Malley and J. Dwyer, J. Chem. Phys. 92 (1988) 3005.
[22] K.J. Farnworth and P.J. O'Malley, J. Phys. Chem. 100 (1996) 1814.
[23] A.D. Becke, J. Chem. Phys. 98 (1993) 5648; P.J. Stephens, F.J. Devlin, M.J. Frisch and C.F. Chabalowski, J. Phys. Chem. 98 (1994) 11623.